

Modeling the Calcium Gate of Cardiac Gap Junction Channel

Chiaki OKA¹, Hiroyuki MATSUDA², Nobuaki SARAI^{1,2}, and Akinori NOMA^{1,3}

¹Cell/Biodynamics Simulation Project, ²Department of Nano-Medicine Merger Education Unit, and ³Department of Physiology and Biophysics, Graduate School of Medicine, Kyoto University, Yoshida-konoe, Sakyo-ku, Kyoto, 606-8501 Japan

Abstract: We addressed the question how Ca^{2+} transients affect gap junction conductance (G_j) during action potential (AP) propagation by constructing a dynamic gap junction model coupled with a cardiac cell model. The kinetics of the Ca^{2+} gate was determined based on published experimental findings that the Hill coefficient for the $[\text{Ca}^{2+}]_i$ – G_j relationship ranges from 3 to 4, indicating multiple ion bindings. It is also suggested that the closure of the Ca^{2+} gate follows a single exponential time course. After adjusting the model parameters, a two-state (open-closed) model, assuming simultaneous ion bindings, well described both the single exponential decay and the $[\text{Ca}^{2+}]_i$ – G_j relationship. Using this gap junction model, 30 cardiac cell models were electrically connected in a one-dimensional cable. However, G_j decreased in a cumulative manner by the repetitive Ca^{2+}

transients, and a conduction block was observed. We found that a reopening of the Ca^{2+} gate is possible only by assuming a sequential ion binding with one rate limiting step in a multistate model. In this model, the gating time constant (τ) has a bell-shaped dependence on $[\text{Ca}^{2+}]_i$, with a peak around the half-maximal concentration of $[\text{Ca}^{2+}]_i$. Here we propose a five-state model including four open states and one closed state, which allows normal AP propagation; namely, the G_j is decreased ~15% by a single Ca^{2+} transient, but well recovers to the control level during diastole. Under the Ca^{2+} -overload condition, however, the conduction velocity is indeed decreased as demonstrated experimentally. This new gap junction model may also be useful in simulations of the ventricular arrhythmia.

Key words: gap junction, mathematical model, heart.

The cardiac gap junctions form intercellular electrical channels between neighboring cells and thereby play an essential role in the action potential (AP) propagation, which triggers a coordinated contraction of cardiac myocytes [1]. The gap junction channels demonstrate opening and closing transitions in response to the potential difference across the gap junction [2] as well as to the intracellular concentrations of Ca^{2+} , Mg^{2+} , protons, and ATP [3–5]. The closure of the channel by intracellular Ca^{2+} concentration ($[\text{Ca}^{2+}]_i$) plays the vital role in protecting intact cells from membrane depolarization by disconnecting the damaged cell (healing over phenomenon) [6]. Namely, the massive diffusion of extracellular Ca^{2+} into the damaged cell causes a closure of gap junction channels. On the other hand, under pathological conditions such as digitalis intoxication or ischemia, an increase in intercellular resistance occurs [7–9] and thereby interferes with AP propagation. Although these qualitative explanations are well accepted, the quantitative aspects have scarcely been clarified. For example, it is still not determined if gap junction conductance (G_j) is affected by the physiological Ca^{2+} transients during the process of the excitation-contraction coupling.

The molecular basis of Ca^{2+} gating is still not clear, but Noma and Tsuboi [4] applied a given concentration of

$[\text{Ca}^{2+}]_i$ to one side of the gap junction and recorded changes in G_j , using paired cells of guinea pig ventricular myocytes. It was found that G_j decreased in a single exponential manner with a time constant (τ) of several seconds, and that the steady state $[\text{Ca}^{2+}]_i$ – G_j relationship was characterized with a half-maximum concentration (EC_{50}) of 0.25 μM and a Hill coefficient of 3.4. The result indicates that the Ca^{2+} gate closes within a physiological range of $[\text{Ca}^{2+}]_i$. However, Weidmann [10] reported that no significant change was detectable in intercellular resistance during a twitch contraction in sheep and calf trabeculae preparation. A possible explanation is that Ca^{2+} transient during a twitch contraction is too fast to induce detectable channel closure. In this study, we aim at constructing a Ca^{2+} gating model of gap junction channels that can reproduce the above experimental findings. Using the novel model, we analyzed the Ca^{2+} gating behavior during the AP propagation. A part of this work has been presented previously in abstract form [11].

METHODS

Dynamic gap junction model. G_j between the neighboring two cells is defined by Eq. 1.

$$G_j = N \cdot g_j \cdot p_{\text{Open}}, \quad (1)$$

Received on Dec 8, 2005; accepted on Jan 27, 2006; released online on Feb 25, 2006; DOI: 10.2170/physiolsci.R2139

Correspondence should be addressed to: Nobuaki Sarai, Department of Nano-Medicine Merger Education Unit, Graduate School of Medicine, Kyoto University, Yoshida-konoe, Sakyo-ku, Kyoto, 606-8501 Japan. Tel: +81-75-753-4353, Fax: +81-75-753-4349, E-mail: sarai@card.med.kyoto-u.ac.jp

where N is the number of gap junction channels, g_j the unitary channel conductance, and $pOpen$ the open probability of the Ca^{2+} gate. To determine g_j , the voltage-dependent gap junction model of Henriquez *et al.* [12], which is based on the mathematical model developed by Vogel and Weingart [13], was used. In brief, a gap junction channel consists of two hemichannels in series. Each one responds to the voltage across hemichannel (V_h) and thereby switches between a low- (L) and a high-conductance state (H). The rate constants μ and γ , which refer to the reactions from L to H and from H to L, respectively, are given by Eq. 2.

$$\begin{aligned}\mu &= \mu_{coef} / (1 + \exp(-|V_h|/V_\mu)) \\ \gamma &= \gamma_{coef} \cdot \exp(-|V_h|/V_\gamma)\end{aligned}\quad (2)$$

where μ_{coef} and γ_{coef} are multipliers and V_μ and V_γ are the slope factors of the voltage-dependence of μ and γ , respectively.

When the channel connects cell $\#i$ and cell $\#(i+1)$, $pOpen$ is expressed as

$$pOpen = y_i \cdot y_{i+1} \quad (3)$$

where y_i and y_{i+1} are the open probabilities of the hemichannels facing $[Ca^{2+}]_i$ of cell $\#i$ and cell $\#(i+1)$, respectively.

Model validation. Two kinds of simulations were performed to verify gap junction models.

(1) Reconstruction of both the $[Ca^{2+}]_i$ - G_j relationship and the time courses of G_j decrease induced by the $[Ca^{2+}]_i$ jump described in the patch clamp experiment: $[Ca^{2+}]_i$ at one side of the gap junctions was jumped from Ca^{2+} -free ($pCa = 9.4$) to a given higher concentration, and the time course of G_j decrease as well as the steady state value of G_j were computed. $[Ca^{2+}]_i$, facing the other side of the gap junctions was set at Ca^{2+} -free.

(2) Simulation of AP propagation: The AP propagation was computed by using a one-dimensional (1-D) cable model, which consisted of 30 ventricular cell models connected to gap junctions. The Kyoto model [14] is used as the cell model. The membrane potential of cell $\#i$ ($V_{m,i}$) in a 1-D cable model is calculated by Eq. 4.

$$C_m \cdot \frac{dV_{m,i}}{dt} + I_{ion,i} = G_{j,i-1} \cdot (V_{m,i} - V_{m,i-1}) - G_{j,i} \cdot (V_{m,i+1} - V_{m,i}) \quad (4)$$

Here C_m and $I_{ion,i}$ are membrane capacitance and total membrane current of cell $\#i$, respectively. $G_{j,i-1}$ and $G_{j,i}$ are the conductance of gap junction model connecting cell $\#(i-1)$ and $\#i$ and connecting cell $\#i$ and cell $\#(i+1)$, respectively. For simplicity, the electrical resistances in the intra- and extracellular medium were neglected. The model was excited at 2.5 Hz by applying a current pulse to cell $\#1$, which was 2.0 ms in duration and 25 nA in amplitude.

The conduction velocity (CV) between cell $\#i$ and cell $\#(i+1)$ was calculated by using Eq. 5:

$$CV = \frac{L_{Cell}}{t_{j_{max},i+1} - t_{j_{max},i}} \quad (5)$$

Here the cell length (L_{Cell}) is set at 100 μm , and $t_{j_{max},i}$ represents the time of the maximum rate of rise of AP in cell $\#i$.

Simulation environment. Simulations were performed on a biological simulation platform called simBio [15]. The differential equations were solved with a discrete time step ($dt = 0.01$ ms), using the fourth-order Runge-Kutta method. All simulations were tested for numeric convergence and accuracy. The source codes of the gap junction models and the Kyoto model can be downloaded from our Web site, <http://www.sim-bio.org>.

RESULTS

Two-state model of the Ca^{2+} gate

We first examined a two-state model (Schema 1) because the single exponential decays were experimentally recorded by applying various $[Ca^{2+}]_i$ to the paired cells (open squares in Fig. 1B).



Here, O and C represent the open and closed states, and α and β are the closing and opening rate constants, respectively. In this model, the open probability of the Ca^{2+} gate of hemichannel $[y(t)]$ obeys Eq. 6:

$$\frac{dy(t)}{dt} = -\alpha \cdot y(t) \cdot [Ca^{2+}]^n + \beta \cdot (1 - y(t)) \quad (6)$$

Equation 6 can be solved as

$$y(t) = (y_0 - y_\infty) \cdot \exp\left(-\frac{t}{\tau}\right) + y_\infty, \quad (7)$$

where y_0 is the open probability at time zero and y is the open probability in the steady state.

$$y_\infty = \frac{\beta}{\alpha[Ca^{2+}]^n + \beta} \quad (8)$$

$$\tau = \frac{1}{\alpha[Ca^{2+}]^n + \beta} \quad (9)$$

Therefore, the rate constants α and β are determined from y and τ determined in experiments.

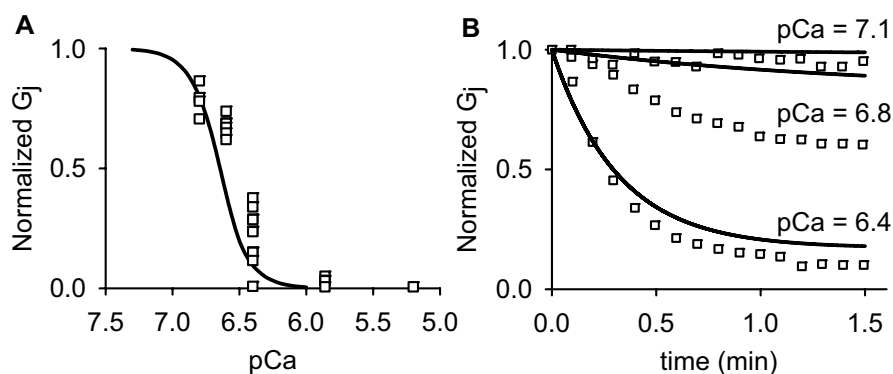


Fig. 1. Comparison of simulation results of the two-state model (solid lines) with the experimental data (open squares) obtained by Noma and Tsuboi [4]. **(A)** $[Ca^{2+}]_i$ -steady state G_j relationship. **(B)** Time courses of G_j decrease at pCa 6.4, 6.8, and 7.1.

$$\alpha = \frac{1 - y_{\infty}}{\tau [Ca^{2+}]^n} \quad (10)$$

$$\beta = \frac{y_{\infty}}{\tau}$$

Noma and Tsuboi reported that y follows the Hill equation, which was characterized with a Hill coefficient (n) of 3.4 and a EC_{50} of 0.251 μM . Using their experimental records, we measured that τ was 19 ms at pCa = 6.4. Thus the rate constants were determined as $\alpha = 1.58 \times 10^7 \text{ mM}^{-3.4} \text{ ms}^{-1}$, $\beta = 9.08 \times 10^{-6} \text{ ms}^{-1}$.

Simulation of Ca^{2+} -gating behavior of the two-state model

Using the two-state model, we plotted the steady-state G_j against pCa (Fig. 1A). Figure 1B shows the time courses of G_j decrease after a jump from zero to various $[Ca^{2+}]_i$. The open squares indicate experimental data, and the solid lines indicate simulation results. The $[Ca^{2+}]_i$ jump at time zero caused the exponential decrease in G_j toward a steady-state level with time constants corresponding to $[Ca^{2+}]_i$. Table 1 shows the simulated τ against experimental data. τ at pCa = 6.8 was about twice as large as the experimental one because rate constants were determined from the data obtained at pCa = 6.4. If rate constants were determined based on the value at pCa = 6.8, τ at pCa = 6.4 was smaller than experimental data. This might indicate that the two-state model is inappropriate for the Ca^{2+} gate.

A more serious limitation of the two-state model was disclosed when the gap junction model was used for simulating the AP propagation. Figure 2A demonstrates CV of the 1-D cable model obtained by applying the stimulus impulse to cell #1. A uniform conduction velocity was ob-

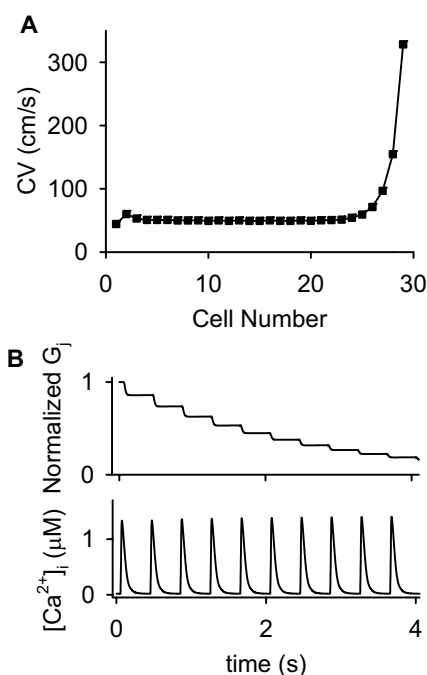


Fig. 2. **(A)** The CV profile along the 1-D cable model of 30 cells. The values of CV between adjacent cells were calculated using Eq. 5. AP was propagated from cell #1, where the stimulus was applied, to cell #30. **(B)** Changes in G_j between cell #15 and #16, and changes in $[Ca^{2+}]_i$ of cell #15 during AP propagation in the 1-D cable model. G_j was normalized at the initial value (2.2 μS) at time zero.

Table 1. Simulated decay time constants compared with experimental data.

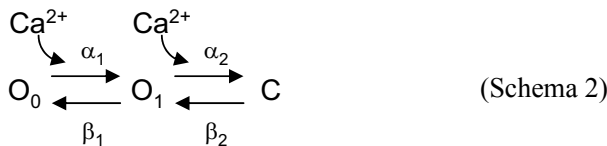
pCa	Two-state model(s)	Five-state model(s)	Experiment(s)
6.4	19.0	25.2	19.0
6.8	65.8	32.3	34.5
7.1	75.1	18.6	Not determined

tained from cell #4 through #23, except at both ends of the cable, where the boundary effect and the stimulus current injection were obvious. CV was shown to be 50 cm/s with the ohmic resistance of 2.2 μS , which well corresponds to the experimental estimation in the paired myocytes [4, 16]. The peak amplitude of the Na^+ current was 10.6 nA during the rising phase of the AP. Then the ohmic conductance was replaced with the two-state gap junction models. To obtain a G_j of 2.2 μS , the number of gap junction channels (N) between cells was set at 30,000. Under this condition, the Ca^{2+} transient of approximately 1.4 μM in amplitude induced the state transition from an open to a closed state in a certain fraction of the channels, resulting in a G_j decrease, as shown in Fig. 2B. The recovery pro-

cess of G_j during diastole is too slow, causing a cumulative decrease in G_j toward an asymptote near zero, and thereby a gradual decrease in CV. This decremental conduction could not be circumvented as far as the two-state model was used. Namely, a recovery of G_j in Eq. 9 can only be accelerated by increasing β at low $[Ca^{2+}]_i$ during diastole. However, this causes a larger step decrease in G_j during the Ca^{2+} transient because the value of α should be proportionally increased to satisfy the constraint of the experimental $[Ca^{2+}]_i$ - G_j relationship. The results definitely indicated that the two-state gap junction model was inappropriate.

$[Ca^{2+}]_i$ - τ relationship in the multistate model

We examined the $[Ca^{2+}]_i$ - τ relationship in the multistate models of Ca^{2+} binding. For simplicity we started with a three-state model shown in Schema 2, where O_0 and O_1 represent the open states and C the closed state.



The probabilities P_{O_0} , P_{O_1} , and P_C of state O_0 , O_1 , and C are given by the following three differential equations.

$$\begin{aligned}
 \frac{dP_{O_0}}{dt} &= -\alpha_1 P_{O_0} [Ca^{2+}] + \beta_1 P_{O_1} \\
 \frac{dP_{O_1}}{dt} &= \alpha_1 P_{O_0} [Ca^{2+}] - \beta_1 P_{O_1} - \alpha_2 P_{O_1} [Ca^{2+}] + \beta_2 P_C \\
 \frac{dP_C}{dt} &= \alpha_2 P_{O_1} [Ca^{2+}] - \beta_2 P_C
 \end{aligned} \quad (11)$$

To reconstruct the single exponential decay of G_j on the $[Ca^{2+}]_i$ jump, we assumed that the first Ca^{2+} binding step is the rate-limiting step, in other words, the binding of the first Ca^{2+} facilitates the following Ca^{2+} binding through a positive allosteric effect. Under this condition, dP_{O_1}/dt can approximate zero; thus P_{O_1} is expressed as

$$P_{O_1} = \frac{\alpha_1 P_{O_0} [Ca^{2+}] + \beta_2 P_C}{\beta_1 + \alpha_2 [Ca^{2+}]} \quad (12)$$

With the use of Eq. 12, dP_C/dt is given by Eq. 13.

$$\frac{dP_C}{dt} = \frac{\alpha_1 \alpha_2 [Ca^{2+}]^2}{\beta_1 + \alpha_2 [Ca^{2+}]} \cdot P_{O_0} - \frac{\beta_1 \beta_2}{\beta_1 + \alpha_2 [Ca^{2+}]} \cdot P_C \quad (13)$$

Equation 13 is mathematically equivalent to the reaction derived from Schema 3. Rate constants (α_{mean} and β_{mean}) and τ are given by Eqs. 14 and 15, respectively.

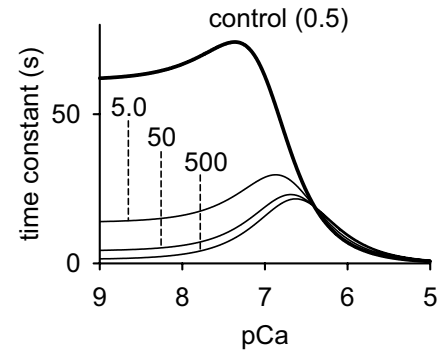
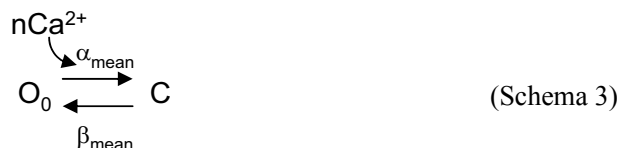


Fig. 3. The τ -pCa relationships at various values of α_2/α_1 (0.5, 5.0, 50, and 500) in the three-state model (Schema 2). Note that τ in the three-state model decreases on both sides of the peak.

$$\alpha_{mean} = \frac{\alpha_1 \alpha_2 [Ca^{2+}]^2}{\beta_1 + \alpha_2 [Ca^{2+}]}, \quad \beta_{mean} = \frac{\beta_1 \beta_2}{\beta_1 + \alpha_2 [Ca^{2+}]} \quad (14)$$

$$\tau = \frac{\beta_1 + \alpha_2 [Ca^{2+}]}{\alpha_1 \alpha_2 [Ca^{2+}]^2 + \beta_1 \beta_2} \quad (15)$$

Shown in a thick line in Fig. 3 is a control $[Ca^{2+}]_i$ - τ curve, where rate constants were defined as $\alpha_1 = 2\alpha_2 = 7.807 \times 10^{-5} \text{ mM}^{-1} \text{ ms}^{-1}$, $2\beta_1 = \beta_2 = 8.135 \times 10^{-9} \text{ ms}^{-1}$ to satisfy the experimental EC_{50} of $0.251 \text{ } \mu\text{M}$ and τ of 19.0 s at $pCa = 6.4$. The peak of the bell-shaped curve is defined by the first-derivative of Eq. 15:

$$\frac{d\tau}{d[Ca^{2+}]} = \frac{-\alpha_2 (\alpha_1 \alpha_2 [Ca^{2+}]^2 + 2\alpha_1 \beta_1 [Ca^{2+}] - \beta_1 \beta_2)}{(\alpha_1 \alpha_2 [Ca^{2+}]^2 + \beta_1 \beta_2)^2} \quad (16)$$

Namely, τ is the maximum at $[Ca^{2+}]_{\tau \max}$, which gives $d\tau/d[Ca^{2+}] = 0$.

$$[Ca^{2+}]_{\tau \max} = \frac{-\alpha_1 \beta_1 + \sqrt{\alpha_1^2 \beta_1^2 + \alpha_1 \alpha_2 \beta_1 \beta_2}}{\alpha_1 \alpha_2} \quad (17)$$

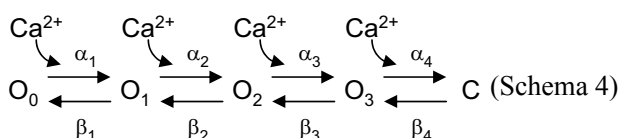
Therefore we concluded that a fast recovery of the Ca^{2+} gate during diastole can be accomplished by a multistate model. In the control model shown in Fig. 3, the Hill coefficient for the $[Ca^{2+}]_i$ - G_j relationship was 1.21. For a higher Hill coefficient with a given EC_{50} , the ratio of α_2/α_1 needs to be increased. Keeping $\beta_2 = \beta_1/2$ and satisfying the experimental EC_{50} of $0.251 \text{ } \mu\text{M}$ and τ of 19.0 s at $pCa = 6.4$, the ratio of α_2/α_1 was systematically changed. With an increasing ratio of α_2/α_1 from 0.5 to 5.0, 50, and 500, the Hill coefficient increased from 1.21 to 1.52, 1.79, and 1.93, respectively, toward the maximum value of 2.0. $[Ca^{2+}]_{\tau \max}$ shifted toward higher concentrations, and τ at lower $[Ca^{2+}]_i$ decreased (Fig. 3).

Table 2. Rate constants in the five-state model.

α_1	2.13	($\text{mM}^{-1} \text{ms}^{-1}$)
α_2	1.96×10^{-1}	($\text{mM}^{-1} \text{ms}^{-1}$)
α_3	2.24	($\text{mM}^{-1} \text{ms}^{-1}$)
α_4	2.09×10^2	($\text{mM}^{-1} \text{ms}^{-1}$)
β_1	3.24×10^{-4}	(ms^{-1})

Development of a five-state model of the Ca^{2+} gate

The results described above indicate that the high co-operation obtained in the experiment (Hill coefficient = 3.4 [4]) is indeed favorable for the rapid recovery of the Ca^{2+} gate during diastole. A five-state model of Ca^{2+} gating was adopted (Schema 4) because binding of at least 4 Ca^{2+} is required to close the hemichannel [4]. The model includes four open states (O_0, O_1, O_2, O_3) and one closed state (C).



The probabilities $P_{O0}, P_{O1}, P_{O2}, P_{O3}$, and P_C at states O_0, O_1, O_2, O_3 , and C, respectively, are determined by the five differential equations (Eq. 18):

$$\begin{aligned}
 \frac{dP_{O0}}{dt} &= -\alpha_1 P_{O0} [\text{Ca}^{2+}] + \beta_1 P_{O1} \\
 \frac{dP_{O1}}{dt} &= \alpha_1 P_{O0} [\text{Ca}^{2+}] - \beta_1 P_{O1} - \alpha_2 P_{O1} [\text{Ca}^{2+}] + \beta_2 P_{O2} \\
 \frac{dP_{O2}}{dt} &= \alpha_2 P_{O1} [\text{Ca}^{2+}] - \beta_2 P_{O2} - \alpha_3 P_{O2} [\text{Ca}^{2+}] + \beta_3 P_{O3} \\
 \frac{dP_{O3}}{dt} &= \alpha_3 P_{O2} [\text{Ca}^{2+}] - \beta_3 P_{O3} - \alpha_4 P_{O3} [\text{Ca}^{2+}] + \beta_4 P_C \\
 \frac{dP_C}{dt} &= \alpha_4 P_{O3} [\text{Ca}^{2+}] - \beta_4 P_C
 \end{aligned} \quad (18)$$

The overall open probability of a single hemichannel (y) is given by:

$$y = P_{O0} + P_{O1} + P_{O2} + P_{O3} \quad (19)$$

The forward rate constants α_1 to α_4 were determined by model fit, and the values of β_1 to β_4 were defined as

$$\beta_2 = 2\beta_1, \beta_3 = 3\beta_1, \beta_4 = 4\beta_1 \quad (20)$$

Since the experimental data are not sufficient to constrain the best fitting procedure, no unique set of solutions was obtained. Only by trial and error was it possible to obtain the parameter set shown in Table 2. Note that the second binding step of Ca^{2+} ($O_1 \rightarrow O_2$) is the slowest one (rate-limiting step) and the following binding steps ($O_2 \rightarrow O_3$ and $O_3 \rightarrow C$) are accelerated ($\alpha_3 = 11.7\alpha_2$, $\alpha_4 = 1090\alpha_2$). As shown in both Fig. 4A and Table 1, the model well reconstructed the $[\text{Ca}^{2+}]_i$ - G_j relationship as well as the time constants. An EC_{50} of $0.25 \mu\text{M}$ and a Hill coefficient of 3.4 were in agreement with the experimental data.

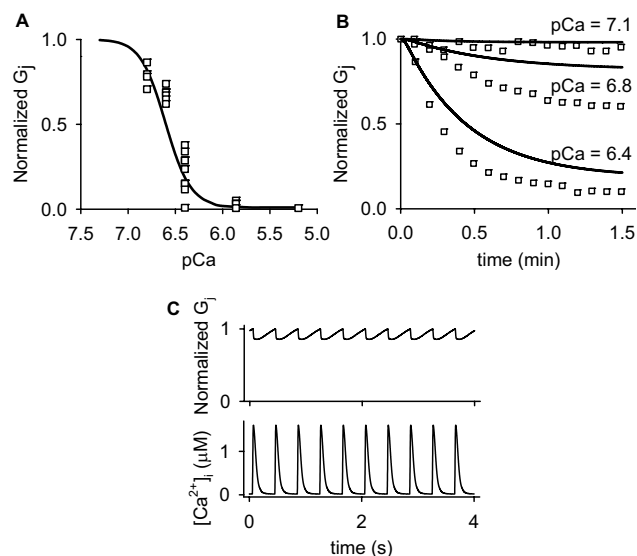


Fig. 4. (A, B) Comparison of simulation results of the five-state model (solid lines) with experimental data (open squares) obtained by Noma and Tsuboi [4]. The steady state $[\text{Ca}^{2+}]_i$ - G_j relationship (A), time courses of G_j decrease at pCa 6.4, 6.8, and 7.1 (B). (C) G_j between cell #15 and #16, and $[\text{Ca}^{2+}]_i$ of cell #15 during AP propagation in the 1-D cable model. G_j was normalized to the diastolic level obtained in the steady state ($p_{\text{Open}} = 0.52$).

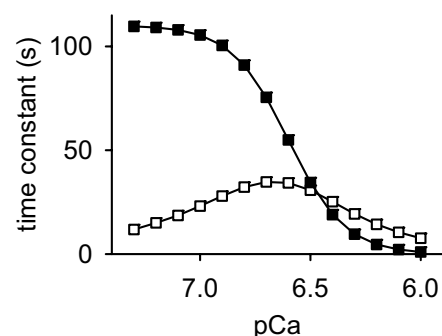


Fig. 5. Relationships between pCa and τ . The open squares are obtained by the five-state gap junction model. The closed squares are obtained by the two-state model.

The values of τ at pCa = 6.4 and 6.8 were closer to experimental data than those of the two-state model (Table 1). In the particular set of experimental G_j decrease in Fig. 4B, the model provided a smaller G_j decrease than in the experiment. We left the fitting as it was because of a variety in the steady state levels of G_j in Fig. 4A.

Figure 4C indicates the time course of G_j between cells #15 and #16 and $[\text{Ca}^{2+}]_i$ of cell #15. Although G_j was decreased by $\sim 15\%$ by the Ca^{2+} transient, it recovered to the initial level during the diastolic period, supporting the sustained AP propagation. τ showed a bell-shaped dependence on $[\text{Ca}^{2+}]_i$ (open squares in Fig. 5). In the steady state, the open probability of the Ca^{2+} gate at diastole was

0.52; then 57,500 of N was required to obtain 50 cm/s of CV. The peak amplitude of $[Ca^{2+}]_i$ was 1.6 μM , which was larger than that in a single cell model (1.4 μM). The increase in the peak $[Ca^{2+}]_i$ was due to an increase of the Ca^{2+} content in the sarcoplasmic reticulum caused by the electrotonic effect from nonexcited cells through gap junctions. Namely, the resting potential of nonexcited cells caused a negative shift of the plateau level of AP, and thereby the L-type Ca^{2+} current was enhanced.

DISCUSSION

The AP propagation has been computed in multidimensional models of cardiac muscle to understand the mechanisms underlying a variety of arrhythmias [17–19]. However, the Ca^{2+} gating of the gap junction channels has not been included, but the cell-to-cell coupling was represented by a given electrical resistance. The goal of our study is to construct a Ca^{2+} gating model of gap junction channels based on experimental findings and to simulate Ca^{2+} gating behavior during AP propagation, not only in the physiological conditions, but also in the pathological conditions.

The simple two-state model of Ca^{2+} gating reproduced the $[Ca^{2+}]_i$ - and time-dependent G_j decrease recorded in experiments, but AP failed to propagate in the cable model. The five-state model, which consists of four open states and one closed state, could successfully reproduce both experimental results. A crucial finding in model development was the difference in the $[Ca^{2+}]_i$ - τ relationship between the two-state model and multistate models. The τ has a sigmoidal dependence on $[Ca^{2+}]_i$ in the two-state model, while a bell-shaped dependence was obtained in the multistate models (Figs. 3 and 5). Thus the recovery of G_j during diastole was possible only with multistate models under the physiological conditions.

Although the five-state model in the present study is not a unique solution because of the limited experimental findings, the model is useful in predicting the gap junction behavior under pathological conditions. An example is shown in Fig. 6, where Ca^{2+} -overload was induced by blocking 50% of the Na^+/K^+ pump in all cell models composing the 1-D cable model. After the Na^+/K^+ pump was suppressed at time zero, a progressive increase in the amplitude of Ca^{2+} transient was observed as a result of $[Na^+]_i$ accumulation via a depression of the Na^+/Ca^{2+} exchanger (Fig. 6, bottom graph). Although the Ca^{2+} transient is augmented, the G_j decreased in a cumulative way because of limited recovery during the diastole (Fig. 6, middle graph). When the diastolic $[Ca^{2+}]_i$ was raised, the beat-to-beat oscillation of G_j disappeared at 43 sec. In parallel to the G_j decrease, average CV between cell #10 and #20 was markedly decreased (Fig. 6, top graph) as experimentally demonstrated by the ouabain exposure to the calf and cow trabeculae [7].

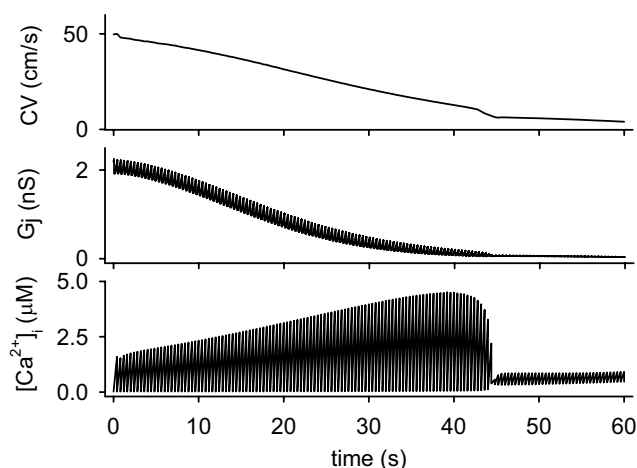


Fig. 6. Simulation of Ca^{2+} -overload condition induced by a 50% block of the Na^+/K^+ pump. The top graph shows the average CV between cell #10 and #20; the middle shows G_j between cell #15 and #16; and the bottom shows $[Ca^{2+}]_i$ in cell #15.

Limitation of the present gap junction model. Under pathological conditions, such as ischemia, the intracellular pH and other metabolites may be changed, which also affect the chemical gate of the gap junction channels. To understand the overall effects of ischemia, a further development of the model is necessary.

The measurements of channel sensitivity to $[Ca^{2+}]_i$ and gate time constants vary among different studies [20–22]. The variation in the experimental measurements may be due to the difference in methods used for inducing change in $[Ca^{2+}]_i$. Noma and Tsuboi [4] achieved a rapid jump of $[Ca^{2+}]_i$ by perforating the cell membrane of paired cells at a given $[Ca^{2+}]$ in bath solution. Thus the relatively fast t and higher Hill coefficient compared with other studies might suggest a better control of $[Ca^{2+}]_i$ near the gap junction. On the other hand, in the conventional method for measuring the gap junction conductance, where $[Ca^{2+}]_i$ was controlled by a limited Ca^{2+} diffusion from the pipette solution during the whole cell clamp condition, $[Ca^{2+}]_i$ might change slowly, and also the steady-state $[Ca^{2+}]_i$ might be overestimated unless the ion flux via cell membrane was completely blocked [23]. However, we cannot exclude the possibility that some regulatory proteins of channel gating were washed out after rupturing the cell membrane of paired cells in Noma and Tsuboi's experiment [4]. Furthermore, in the experiment of Noma and Tsuboi, the time course of G_j decrease at the beginning of applying test solutions of various pCa might also be contaminated by a diffusion delay of Ca^{2+} over the distance from the perforated membrane to the vicinity of the gap junctional channels.

This study was supported by the Leading Project for Biosimulation and a Grant-in-Aid 17700393 for Scientific Research from the Ministry of Education, Culture, Sports, Science and Technology of Japan.

REFERENCES

1. Rohr S. Role of gap junctions in the propagation of the cardiac action potential. *Cardiovasc Res.* 2004;62:309-22.
2. Bukauskas FF, Verselis VK. Gap junction channel gating. *Biochim Biophys Acta.* 2004;1662: 42-60.
3. Peracchia C. Chemical gating of gap junction channels; roles of calcium, pH and calmodulin. *Biochim Biophys Acta.* 2004;1662: 61-80.
4. Noma A, Tsuboi N. Dependence of junctional conductance on proton, calcium and magnesium ions in cardiac paired cells of guinea-pig. *J Physiol.* 1987;382:193-211.
5. Sugiura H, Toyama J, Tsuboi N, Kamiya K, Kodama I. ATP directly affects junctional conductance between paired ventricular myocytes isolated from guinea pig heart. *Circ Res.* 1990;66:1095-102.
6. Deleze J. The recovery of resting potential and input resistance in sheep heart injured by knife or laser. *J Physiol.* 1970;208:547-62.
7. Weingart R. The actions of ouabain on intercellular coupling and conduction velocity in mammalian ventricular muscle. *J Physiol.* 1977;264:341-65.
8. Kleber AG, Riegger CB, Janse MJ. Electrical uncoupling and increase of extracellular resistance after induction of ischemia in isolated, arterially perfused rabbit papillary muscle. *Circ Res.* 1987;61:271-9.
9. Hiramatsu Y, Buchanan JW, Jr., Knisley SB, Koch GG, Kropp S, Gettes LS. Influence of rate-dependent cellular uncoupling on conduction change during simulated ischemia in guinea pig papillary muscles: effect of verapamil. *Circ Res.* 1989;65:95-102.
10. Weidmann S. Electrical constants of trabecular muscle from mammalian heart. *J Physiol.* 1970;210:1041-54.
11. Oka C, Matsuda H, Sarai N, Matsuoka S, Noma A. Dependency of myocardial function on gap junction conductance. *Jpn J Physiol* 55 Suppl. 2005:S90.
12. Henriquez AP, Vogel R, Muller-Borer BJ, Henriquez CS, Weingart R, Cascio WE. Influence of dynamic gap junction resistance on impulse propagation in ventricular myocardium: a computer simulation study. *Biophys J.* 2001;81:2112-21.
13. Vogel R, Weingart R. Mathematical model of vertebrate gap junctions derived from electrical measurements on homotypic and heterotypic channels. *J Physiol.* 1998;510 (Pt 1):177-89.
14. Matsuoka S, Sarai N, Kuratomi S, Ono K, Noma A. Role of individual ionic current systems in ventricular cells hypothesized by a model study. *Jpn J Physiol.* 2003;53:105-23.
15. Sarai N, Matsuoka S, Noma A. simBio: A Java package for the development of detailed cell models. *Prog Biophys Mol Biol.* 2006; 90:360-77.
16. Kameyama M. Electrical coupling between ventricular paired cells isolated from guinea-pig heart. *J Physiol.* 1983;336:345-57.
17. Beaumont J, Davidenko N, Davidenko JM, Jalife J. Spiral waves in two-dimensional models of ventricular muscle: formation of a stationary core. *Biophys J* 1998;75: 1-14.
18. Clayton RH, Bailey A, Biktashev VN, Holden AV. Re-entrant cardiac arrhythmias in computational models of long QT myocardium. *J Theor Biol.* 2001;208:215-25.
19. Sampson KJ, Henriquez CS. Electrotonic influences on action potential duration dispersion in small hearts: a simulation study. *Am J Physiol Heart Circ Physiol.* 2005;289:H350-60.
20. Maurer P, Weingart R. Cell pairs isolated from adult guinea pig and rat hearts: effects of $[Ca^{2+}]_i$ on nexal membrane resistance. *Pflugers Arch.* 1987;409:394-402.
21. Lazrak A, Peracchia C. Gap junction gating sensitivity to physiological internal calcium regardless of pH in Novikoff hepatoma cells. *Biophys J.* 1993;65: 2002-12.
22. Firek L, Weingart R. Modification of gap junction conductance by divalent cations and protons in neonatal rat heart cells. *J Mol Cell Cardiol.* 1995;27:1633-43.
23. Mathias RT, Cohen IS, Oliva C. Limitations of the whole cell patch clamp technique in the control of intracellular concentrations. *Biophys J* 1990;58: 759-70.